České vysoké učení technické v Praze
Fakulta jaderná a fyzikálně inženýrská

Bakalářská práce

Produkce kvarkónií v jádro-jaderných srážkách na RHIC a LHC

Praha, 2009

Autor: Olga Hájková

Vedoucí práce: Mgr. Jaroslav Bielčík, Ph.D.

Czech Technical University in Prague
Faculty of Nuclear Sciences and Physical Engineering

Bachelor's Thesis

Quarkonia production in heavy-ion collision at RHIC and LHC

Prague, 2009

Author: Olga Hájková

Supervisor: Mgr. Jaroslav Bielčík, Ph.D.

Název: Produkce kvarkónií v jádro-jaderných srážkách na RHIC a LHC
Autor: Olga Hájková
Obor: Experimentální jaderná fyzika
Druh práce: Bakalářská práce
Vedoucí práce: Mgr. Jaroslav Bielčík, Ph.D., Katedra fyziky, FJFI, ČVUT v Praze.
Abstrakt: Produkce J/ψ mezonu je v kvark-gluonové plazmě potlačena z důvodu barevného odstínění, toto potlačení se považuje za nejvýznamnější známku vzniku QGP. Ve srážkách d+Au při energii $\sqrt{s}$=200 GeV byl zrekonstruován signál J/ψ v e^+e^- kanálu se signifikancí 4.2σ.
Klíčová slova: těžké kvarky , charmonia, STAR, srážky těžkých iontů, kvark gluonové plazma, J/ψ mezon

Title: Quarkonia production in heavy-ion collision at RHIC and LHC
Abstract: Since the J/ψ production in QGP is expected to be suppressed due to the color screening, the suppression of the J/ψ yield has been considered as the most promising signature of the QGP formation. Such high temperature and high density state is expected to have been realized in the early universe. The J/ψ productions in d+Au collisions at the center of mass energy per nucleon pair $\sqrt{s}$=200 GeV have been studied at the STAR experiment at the Relativistic Heavy Ion Collider at the Brookhaven National Laboratory.
Key words: heavy quarks, charmonia, STAR, heavy ion collisions, quark gluon plasma, J/ψ meson

Acknowledgements

I would like to express my gratitude to all those who gave me the possibility to complete this work. I am very grateful to my supervisor Jaroslav Bielčík for his invaluable help, advice and support during creation of this work. I am also very thankful to Jan Kapitán, David Tlustý and Miroslav Krůs for their important advices and helpful information. Last but not least I would like to thank to my father Vladimír Rogalewicz for languages consultations.

Contents

Introduction

Quarks and leptons are fundamental constituents of matter (Fig.1). Quarks are constituents of hadrons: mesons and baryons. There are six different flavors of quarks: up, down, strange, charm, beauty and top. Quarks can exist only inside hadrons because they are confined there. Beside the other quantum numbers quarks carry also a color charge that is associated with the strong interaction.

Similarly to quarks, there are six types of leptons: electrons, muons, tauons, and corresponding neutrinos. The electron, the muon, and the tau carry a negative charge, whereas the three neutrinos carry no charge. Charged leptons interact via electromagnetic and weak forces, while for neutral leptons only the weak interaction has been observed.

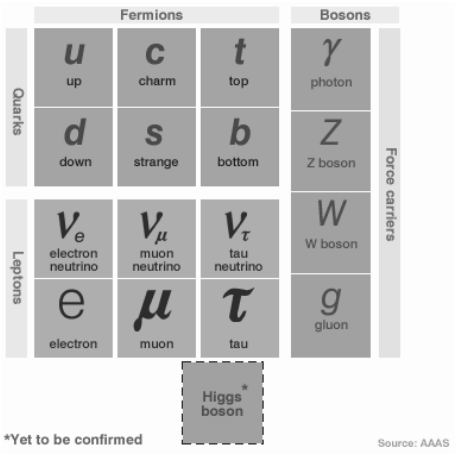

Figure 1: Fundamental particles of a Standard model. Each particle has also its antiparticle.

The third group of elementary particles are interaction carrier particles: gluons, $W^{\pm}$ mesons, Z^0 mesons and photons.

The individual category is the Higgs boson that is assumed to be responsible for particle properties associated with mass. The Higgs boson has not yet been observed. Every particle in Fig. 1 has its antiparticle.

The objective of the high energy physics is the detection and measurement of the properties and behavior of these fundamental particles, along with the understanding of the forces acting among them. These four forces are: the electromagnetic force, the strong force, the weak force, and gravitation.

This work is about heavy ion physics. In heavy ion physics by the means of nucleus-nucleus collisions, the properties of the hot and dense nuclear matter is investigated.

1 Heavy ion physics

1.1 QGP and its signatures

Quantum Chromodynamics (QCD) is a theory of strong interaction between quarks and gluons. Quarks have a quantum number called color and they are confined by gluons in colorless hadrons. There are three possible colors of quarks: red, blue and green, and three possible anticolors of antiquarks. The interaction between two coloured particles is characterized by the strong interaction coupling constant α_s:

$$\alpha_s = \frac{12\pi}{(33-2N_f)\ln(\frac{Q^2}{\lambda_{QCD}})} \tag{1}$$

where Q^2 is four momentum transfer, N_f is the number of quark flavours and λ_{QCD} is the typical QCD scale (λ_{QCD} 0.2GeV). The coupling constant α_s for the strong force becomes smaller at shorter distances. This effect is known as asymptotic freedom. Another important effect is the color confinement. The confinement means that the force between quarks is stronger at larger distances and quarks seem to remain confined at small distances. The coupling constant α_s decreases with an increase in momentum transfer and decreases in the environment of high temperature and/or densities too. When the system reaches the critical temperature, the color confinement is broken and matter passes through phase transition from the confined nuclear matter to the deconfined state. This is predicted from calculations on lattice QCD. A phase diagram of hadronic matter shown in Fig. 2 as a function of temperature and the baryon density. The assumed phase transition line between hadron gas and quark gluon plasma (QGP) is denoted.

Quark gluon plasma is a new state of matter which is composed of deconfined quarks and gluons. QGP is believed to exist in the early universe, about 10^{-6} second after the Big Bang. High energy heavy ion collisions provide a possibility to produce QGP in the laboratory. Current calculations show that the transition happens around the critical temperature $T_c = 150-180$MeV, which corresponds to an energy density of about $0.3 - 1.0$GeV/fm^3[1].

Even if QGP is produced in a laboratory, its identification is difficult because of its very short lifetime. Its impossible to directly observe its thermodynamics variables. So, its necessary to rely on indirect measurements of QGP formation. Certain signatures of the phase transition could allow us to establish whether the matter is deconfined or not. Observable signatures in high energy heavy ion collisions could be divided into three classes: hard, electromagnetic and soft probes. Hard probes that included J/ψ suppression are of the most interest of this work.

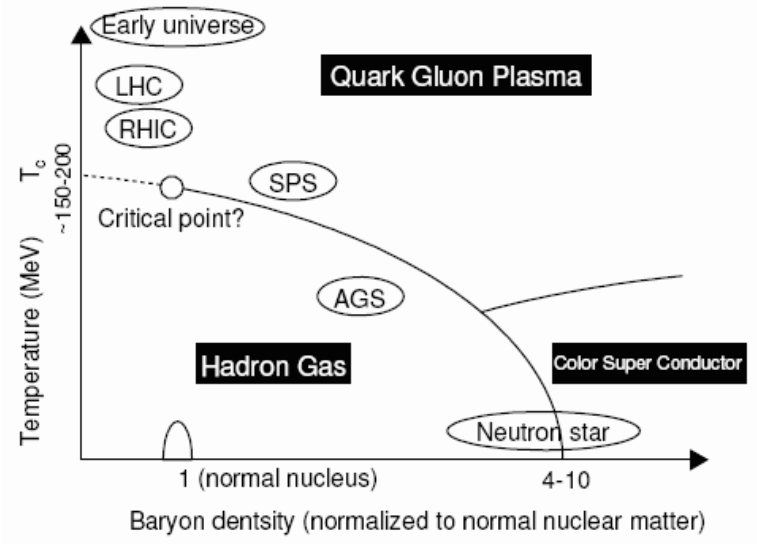

Figure 2: A phase diagram of matter. Assumed phase transition lines are denoted[2].

As mentioned above also the J/ψ suppression research has been considered as one of the most promising signatures for QGP formation since Matsui and Satz proposed it [3]. Due to color screening of the surrounding nuclear matter a J/ψ are expected to disassociate under certain conditions. Therefore, J/ψ has been used as a tool of searching for QGP formation in heavy ion collisions.

1.2 Collision geometry and centrality

Geometry of two colliding nuclei is very important for collision dynamics. As illustrated in Fig.3, the nucleons in collision can be classified into two groups, spectators and participants. The nucleons in the overlap region participate on the collision, so they are called participants. The nucleons in the other nucleus region are called spectators.

The main parameter of colliding nuclei is the impact parameter b . The impact parameter denotes the sizes of spectator and participant groups. This way, we can speak about central and peripheral collisions. If the impact parameter b is nearly zero or very small, almost all nucleons participate in the collision, and the collision is called central. When the impact parameter is large, the collision is called peripheral. The central and peripheral collisions are shown in Fig.4.

1.3 Space-time evolution of matter

The evolution of matter created in high-energy heavy ion collisions can be illustrated by the space-time diagram (Fig.5), with the longitudinal coordinate z and

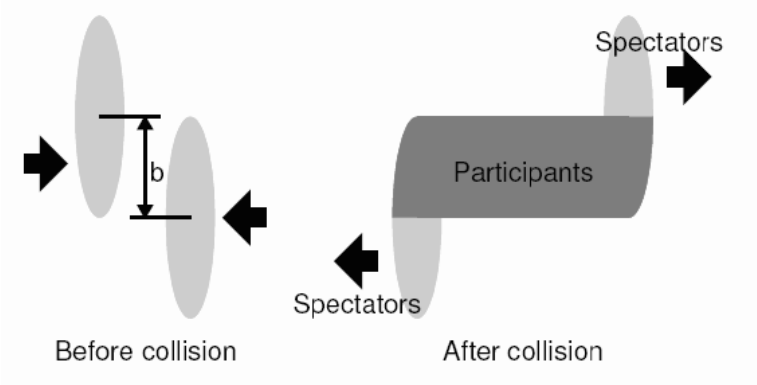

Figure 3: Spectators and participants - active and passive regions of colliding nuclei [2].

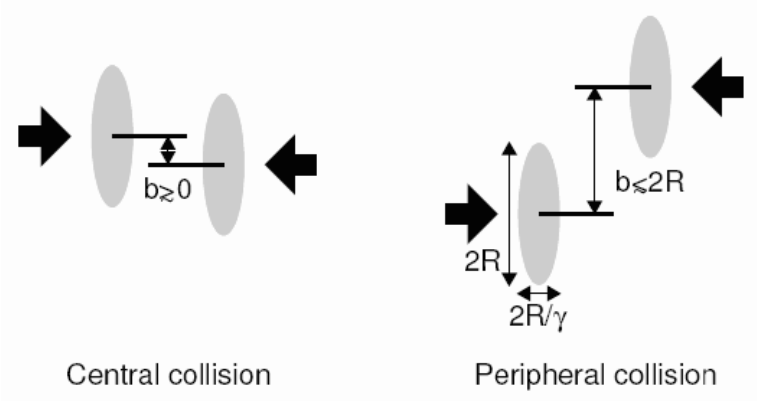

Figure 4: A central collision with a small impact parameter on the left and a peripheral collision with a large impact parameter on the right [2].

transversal coordinate t. It may be viewed as evolving through the following stages that are expected to exist from the initial collision to the final hadronic phase: It is assumed that the space-time evolution depends only on the proper time $\tau = \sqrt{t^2 - z^2}$:

1)At the proper time $\tau = 0$ a huge amount of energy is disengaged in a tiny volume. The expected energy density is high enough to form the deconfinned matter of quarks and gluons. Matter in this stage is not in the thermal equilibrium. The dynamics in this phase could be described by a cascade of colliding partons.

2) Deconfined state of partons in thermal equilibrium. This phase is called the QGP stage. The QGP then evolves like fluid, expands and cools down with according to hydrodynamic laws.

3)At $\tau = \tau_c$ the system has reached the critical temperature T_c and starts to hadronize. If the transition is first order, matter passes through the mixed phase consisting of gluons, quarks and hadrons.

4)The hadronization of the system is finishing and hadrons are interacting with each other till the temperature drops to the freeze-out temperature.

5)At the freeze-out temperature hadrons finish interacting and leave the collision region.

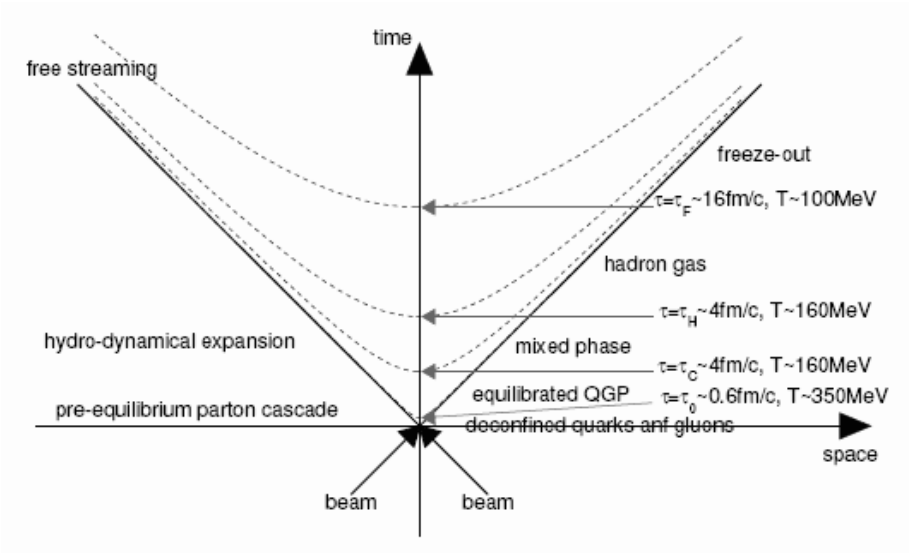

Figure 5: Time space evolution of matter created in high energy heavy ion collisions [2].

1.4 The binary collision and the nuclear modification factor

The binary collision is an interaction between two free particles, in terms of heavy ion collisions it is an interaction between two nucleons. The nuclear modification factor R_{AA} quantifies the effect of heavy ion collisions compared to p+p collisions scaled by the mean number of binary collisions in the heavy ion collision sample.

2 Charmonium system and production mechanism

2.1 J/ψ discovery

The J/ψ meson was discovered in 1974 in two independent laboratories simultaneously. At Stanford at SPEAR collider in e^+e^- anihilation, by Burton Richter and at Brookhaven National Laboratory at the alternating gradient synchrotron (AGS) in p+Be collisions, by Samuel Ting. This new particle decayed slowly and did not fit into the framework of up, down, and strange quarks. The J/ψ discovery was the first firm experimental evidence for the fourth quark. Richter and Ting shared the Nobel Prize for their discovery in 1976.

2.2 Charmonia family

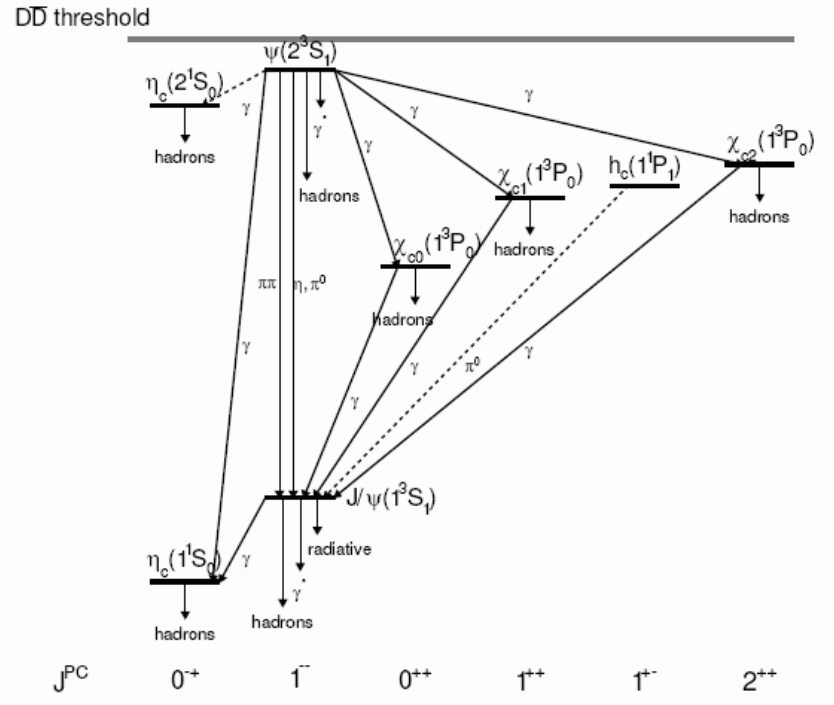

Figure 6: Charmonium model, the current state of knowledge of the charmonium system. The dashed line denotes uncertain transitions [2].

Quarkonium is a bound state of a heavy quark and antiquark pair. Quarkonium composed of a charm quark and antiquark pair is called charmonium, and quarkonium composed of a bottom quark-antiquark pair is called bottomonium. The schema of charmonium current state knowledge is illustrated in

Fig.6. Charmonium states can be classify by their principal quantum number n. This schema shows charmonia in the ground state (n=1) the J/ψ meson and ν_c, and charmonia in the excited state (n=2) the ψ' meson and three states of χ_c. Excited state of charmonia could feed-down to J/ψ with emission of the photon. Feed-down means a decay in to the J/ψ meson and photon.

J/ψ seem to be the most famous charmonium. Properties of the J/ψ meson and the other charmonium bound states are shown in Table1.

Particle	Mass [MeV/c^2]	Width[MeV/c^2]	Decay mode	Branching ratio
			hadrons	87.7±0.5
J/ψ	3097	0.093	e^+e^-	5.94±0.10
			$\mu^+\mu^-$	5.93±0.10
χ_0	3415	10.4	J/$\psi+\gamma$	1.30±0.10
χ_1	3511	0.89	J/$\psi+\gamma$	35.6±1.9
χ_2	3556	2.06	J/$\psi+\gamma$	20.2±1.0
			hadrons	97.9±0.3
ψ'	3686	0.277	J/$\psi+X$	56.1±0.9
			e^+e^-	0.74±0.18
			$\mu^+\mu^-$	0.73±0.18

Table 1: Properties of charmonia bound states: mass, width, decay modes and branching ratio

2.3 Theoretical model of charmonia production

Production of J/ψ from initial partons is divided into two steps. The first step is a $c\bar{c}$ pair production in hard scattering of the initial partons and the second one is hadronization into J/ψ from the $c\bar{c}$ pair. A more complicated part is obtaining the bound state from a $q\bar{q}$ pair (step 2), especially if the bound state is to be produced with the right angular momentum and spin quantum numbers. There are several theoretical models employed for quarkonium production: the color singled model (CSM), the color evaporation model (CEM), the color octet model (COM). However, no of these models seceded to make universal description of the quarkonium production. These models are briefly explained in the following section.

a) Color singled model

The CMS was first proposed shortly after J/ψ discovery. It requires the colorless $c\bar{c}$ pair to be created with the same quantum numbers as the J/ψ meson. Fig.7 shows an example of the lowest order diagram of J/ψ production in the CSM, where the $c\bar{c}$ pair has $^3S_1$ and should be colorless as the J/ψ.

To conserve C parity, hard gluon emission is necessary in the color singlet model. This model can describe the J/ψ production cross section in the photo-

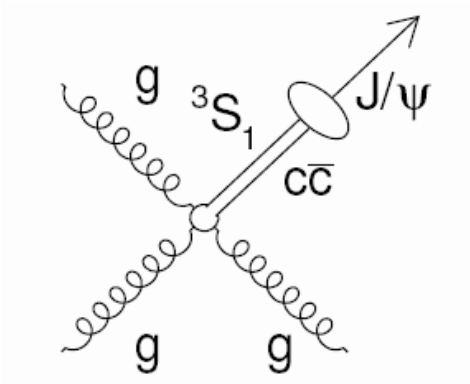

Figure 7: An example of the lowest order diagram for direct a J/ψ production from gluon (g) fusion with the color singlet model. The $c\bar{c}$ pair is in the color singlet state [1].

production, but failed to explain the p_T differential cross section in $p+\bar{p}$ collisions at the Tevatron at the FNAL [4].

b) Color evaporation model

The CEP was first proposed in 1977. In the CEM model the quarkonium production is processed in the same way as open heavy quark production with the restriction that the $c\bar{c}$ mass must be bellow the $D\bar{D}$ thrashold [5]. The CEM does not have any constraints on color or other quantum numbers for the $c\bar{c}$ pair. The CEM assumes that the $c\bar{c}$ pair neutralizes its color by an interaction with collision-induced color field, called 'color evaporation'. In the CEM the J/ψ is formed through multiple soft gluon emissions that destroy the information on quantum numbers of the $c\bar{c}$ pair as shown in Fig.8.

The CEM describes a total hadro-production and photo-production of J/ψ at lower energies. The CEM predicts zero polarization of the J/ψ meson that is consistent in the lower p_T region, but that is not consistent in the intermediate and high p_T regions[1].

c) Color octet model

The color octet model (COM) was developed in the 1990's based on the non-relativistic QCD (NRQCD) framework[5]. The COM allows a J/ψ formation from a color octet $c\bar{c}$ pair with one or few soft gluons emissions. An example of the COM is shown in Fig.9. The COM has successfully reproduced the p_T distribution in $p + \bar{p}$ collisions and the total cross section at lower-energy experiments[1]. On the other hand, the COM predicts large transverse polarization, while large longitudinal polarization is observed experimentally.

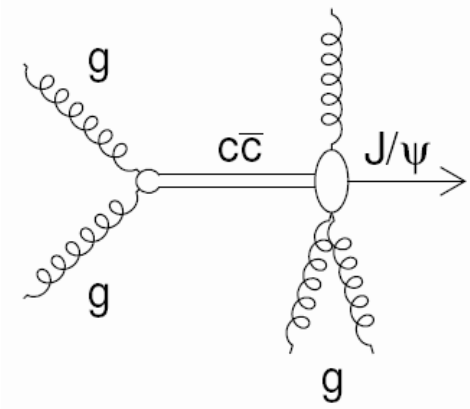

Figure 8: An example of the lowest order diagram for the direct J/ψ production from a gluon fusion with the color evaporation model [1].

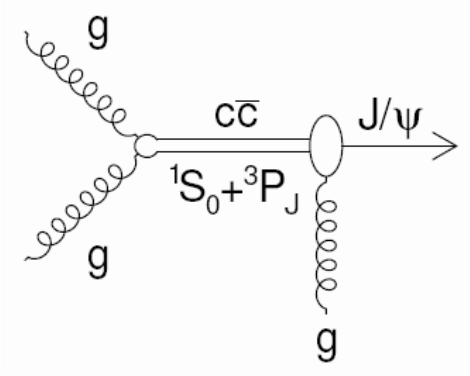

Figure 9: An example of the lowest order diagram for the direct J/ψ production from the gluon fusion with the COM [1].

2.4 Different channels of J/ψ production

J/ψ mesons actually measured in hadron-hadron collisions can have four different origins: a direct production of J/ψ, feed down from three χ_c states, feed down from a ψ' state, and a production from the decay of a bottom quark.

The part of measured J/ψs from three χ_c states decays is represented by the ratio $R_{\chi c}$, and J/ψs produced from the ψ' state are represented by the ratio R'_{ψ} defined as follows:

$$\mathrm{R}_{\chi c}=\frac{1}{\sigma_{J/\psi}}\sum_{i=0}^{2} BR(\chi_{ci} \to J/\psi+\gamma)\sigma_{\chi ci}$$

$$\mathrm{R}_{\psi'}=\frac{\sigma_{\psi'}}{\sigma_{J/\psi}} BR(\psi' \to J/\psi+X) \tag{2}$$

where $\sigma_J/_\psi$ is a J/ψ cross section, $BR(\chi_c \to J/\psi+\gamma)$ is a branching ratio of the $\chi_c \to J/\psi$ decay, and $BR(\psi' \to J/\psi+X)$ is a branching ratio of the $\psi' \to J/\psi$ decay. The average value of $R_{\chi c}$ is about 0.3, and $R_{\psi'}$ is assumed to be less than 0.1 [2]. Finally, the fraction of the J/ψ production from a bottom quark decay is represented by the ratio R_b and is about 0.014 [2]. To sum it up, the contributions to the J/ψ production from the 4 origins are:

1.Directly produced J/ψs are about 0.6

2.J/ψs produced from three χ_c states decay are about 0.3

3.J/ψs produced from the ψ' decay are about 0.1

4.J/ψs produced from the bottom quark decay are about 0.01

2.5 J/ψ production in hadron-hadron collisions

Since charm quarks are heavy, the production of charm quarks takes place only at the beginning of the collision. J/ψ may be formed before QGP formation. On that account, medium effect on the J/ψ production can be categorized into two groups: cold nuclear matter effects and final state effects.

Cold nuclear matter effects take place before the QGP formation. The possible contribution to the modification of the J/ψ production are gluon shadowing and nuclear absorption.

Final state effects take place after the QGP formation. There are following contributions to the modification of the J/ψ production: color screening in QGP, recombination of J/ψs from uncorrelated $c\bar{c}$ pairs, and the J/ψ interaction with secondary comovering hadrons. The final state effects are briefly described in the following section.

Color screening

The potential of a $q\bar{q}$ pair in vacuum can be described as follows:

$$V(r,T=0)=-\frac{4}{3}\frac{\alpha_s(r)}{r}+\sigma r \tag{3}$$

where r is the distance between quark and antiquark, σ is the string tension coefficient, and q is a color charge. In finite temperatures this potential is modified due to color screening:

$$V(r,T)=-\frac{\alpha_{eff}}{r}exp[-\frac{r}{\lambda_D(T)}]+\sigma\lambda_D(T)[1-\exp(-\frac{r}{\lambda_D(T)})] \tag{4}$$

where $\lambda_D(T)$ is the Debye screening lenght. The Debye screening lenght depends on the temperature and decreases with its increase. It can be evaluated as follows:

$$\lambda_D(T)=\frac{1}{\sqrt{(\frac{N_c}{3}\frac{N_f}{6})g^2T}} \tag{5}$$

where N_c is the degree of color freedom, N_f is the number of quark flavors, $g^2 = 4\pi\alpha_{eff}$, and T is the matter temperature. When the Debye screening length is smaller than the charmonium radius, quark and antiquark cannot stay longer in the bound state. For the QGP ($N_c = 3$, $N_f = 3$, $T = 200MeV$), the screening length is $\lambda_D = 0.33$ fm [4]. Since the J/ψ radius is 0.453fm, it predicates that $c\bar{c}$ pairs cannot stay in the bound state in the QGP at the temperature $T = 200MeV$.

J/ψ recombination

J/ψ production could be enhanced due to uncorrelated $c\bar{c}$ pairs recombination. This scenario is predicted at RHIC energies, and it is derived from the assumption that the number of recombined charmonia are approximately proportional to N_c^2/N_h, where N_c is the number of created charm quarks, and N_h is the number of produced hadrons. The charm production N_c increases faster with $\sqrt{s}$, and scales with the number of inelastic nucleon-nucleon collisions, while N_h scales with the number of participant nucleons. Since the number of nucleon-nucleon collisions is sufficiently higher in more central collisions than the number of participant nucleons at RHIC energy, N_c^2/N_h leads to a higher value at a higher collision energy and in more central collisions. Hence, this effect cannot be negligible at the RHIC energy.

Comover interactions

An additional absorption of J/ψ by secondary hadrons called comovers occurs in the hadronic phase. The survival probability of J/ψ can be expressed as follows:

$$S_{CO} = exp(-\int d\tau \rho_{CO}(\tau)\sigma_{CO}v) \tag{6}$$

where τ is time, ρ_{CO} is the comovers density, v is the relative velocity between the J/ψ and a secondary hadron, and σ_{CO} is a cross section of the J/ψ absorption by comovers [5].

3 Experimental setup

3.1 The Relativistic Heavy Ion Collider

The Relativistic Heavy Ion Collider (RHIC) is located at the Brookhaven National Laboratory in Upton, New York. The RHIC started its operation in 2000. Research at the RHIC is focuses on the study of a quark gluon plasma, the primordial state of matter that existed in the early universe. The whole RHIC complex is illustrated in Fig.10. The RHIC is an intersection storage ring (ISR) particle accelerator composed of two independent rings. The RHIC has a circumference of 3834 m and 6 intersection points where particles collide. Originally there were 4 experiments at intersection points: STAR, PHENIX, BRAHMS and PHOBOS. BRAHMS and PHOBOS completed their program already. The maximum center of mass energy per nucleon-nucleon pair for Au+Au collisions is $\sqrt{s} = 200$ GeV. It can also collide p+p up to 500GeV and d+Au, Cu+Cu up to 200GeV.

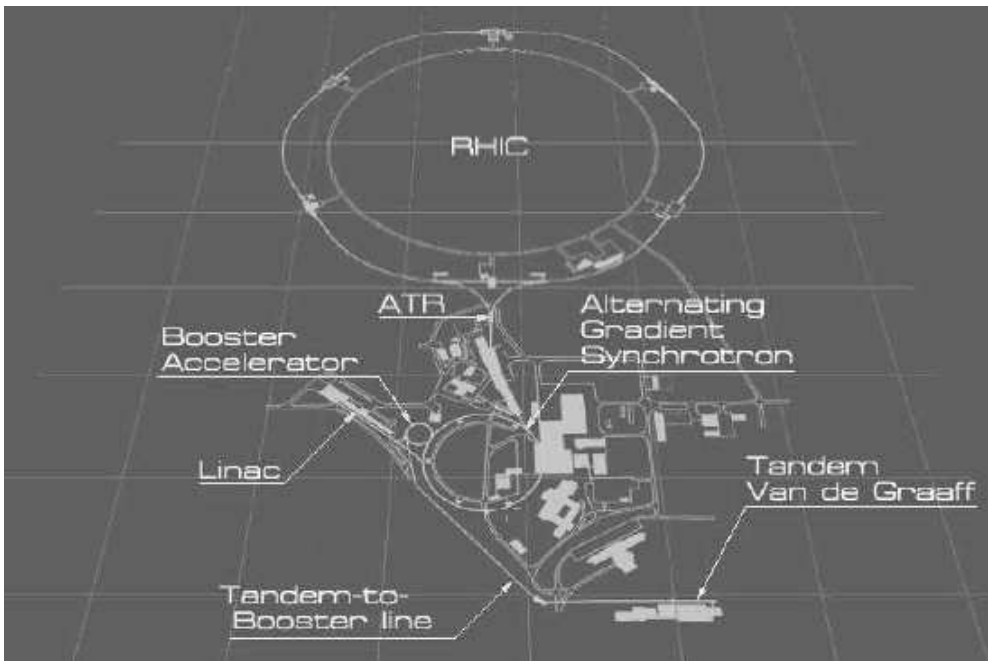

Figure 10: A schematic view of the RHIC complex [6].

Before reaching the RHIC storage ring, each particle passes through several stages illustrated in Fig.10. Heavy ions started their acceleration in the Tandem Van de Graaf. Then passed through the Tandem-to-Booster line, the Booster synchrotron, the Alternating Gradient Synchrotron (AGS), and the AGS-To-

RHIC (ATR) transfer line, consequently. At the end of this process, ion bunches are sent by switching magnets to the one of two beam lines. Finally, the bunches are colliding into one of four interaction point.

3.2 STAR

The Solenoidal Tracker at the RHIC (STAR) is a massive detector that was designed especially for a study of the hadron production and search for signatures of the quark gluon plasma formation and its properties. The principal constituents of the STAR experiment are a solenoidal magnet (0.5T maximally) and a Time Projection Chamber (TPC) which is used as a primary tracking device. The STAR detector schema is shown in Fig. 11. This work has been performed in the STAR collaboration.

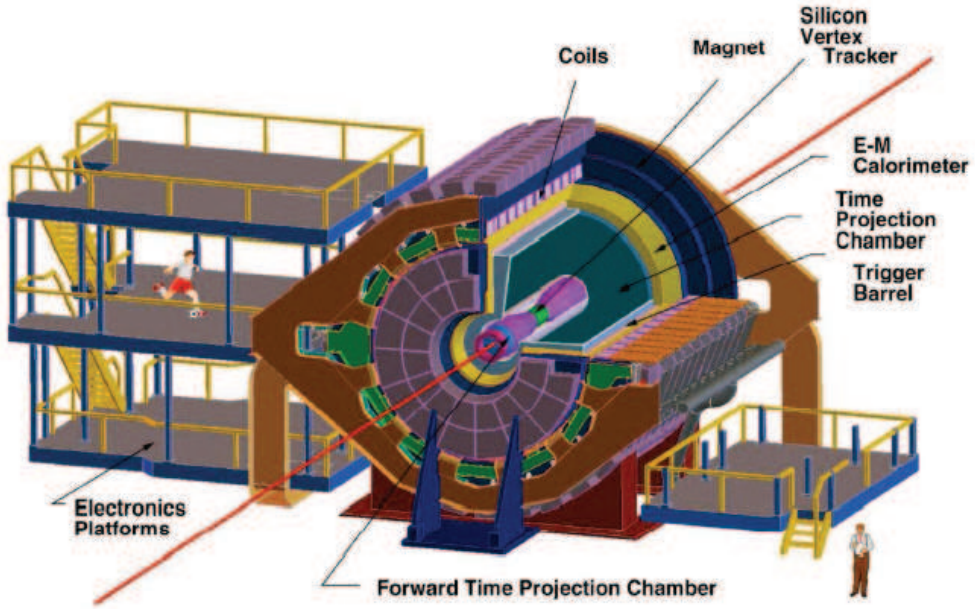

Figure 11: The experimental setup of the STAR detector [7].

Solenoid magnet

The present design of the magnet produces a nearly uniform field over the operating range $0.25 < |Bz| < 0.5$ T parallel to the beam direction over the entire TPC volume.

Time Projection Chamber (TPC)

The TPC (illustrated in Fig. 12) is a central element located in the solenoidal magnet and having 4.2 m along the beam axis and 4 m in diameter. The TPC registers tracks of particles, measures their momentum, and identifies particles via the ionization loss (dE/dx). Its acceptance covers ± 1.8 units of pseudo-rapidity through the full azimuthal angle. Particles are identified over a momentum range from 100 MeV/c to move than 1 GeV/c, and momenta are measured over a range of 100 MeV/c to 30 GeV/c [15].

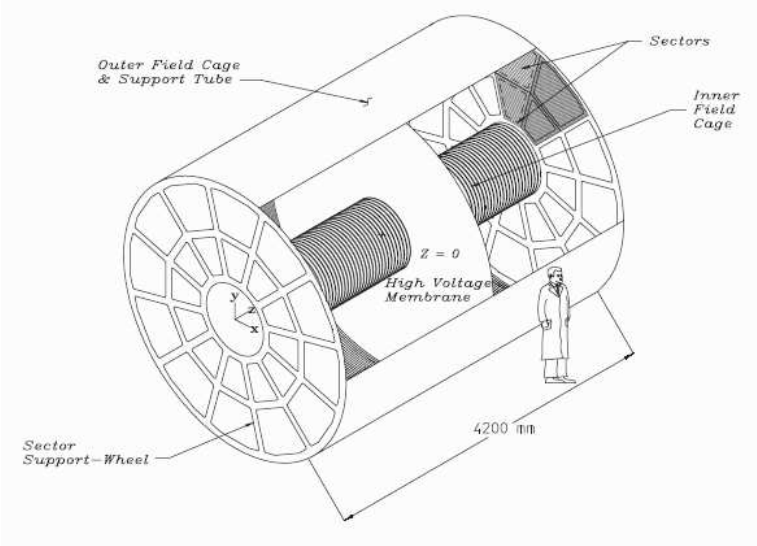

Figure 12: STAR TPC schema [15].

The TPC is an empty volume filled with an argon+diomethan gas mixture, in a well defined, uniform, electric field of 135 V/cm . This gas was chosen with respect to its minimum attenuation of the drifting electrons. The trajectories of primary ionizing particles are reconstructed from released secondary electrons drifting to the readout end caps at the ends of the chamber.

The uniform electric field required to drift the electrons is defined by a thin conductive membrane at the center of the TPC. The tracks (x,y coordinates) are reconstructed from the pad signals and from the electron drift time (z coordinate). The dE/dx is calculated from the energy loss measured on up to 45 pad rows.

The Barrel Electromagnetic Calorimeter (BEMC)

The BEMC is included of 120 calorimeter modules, each of them is segmented into 40 towers. Every tower is oriented in the direction of the interaction point. The inner surface of the BEMC has a radius of about 220cm and the outer

radius is about 250 cm.

The BEMC provides large acceptance for photons, electrons and π^0 mesons. All these measurements require precise electromagnetic shower reconstruction with high spatial resolution. The shower maximum detector (SMD) was implemented within the BEMC. The SMD provides this resolution of shower distributions.

Other components

Other STAR components are: the Forward Time Projection Chamber (FTPC) that enhances the acceptance of the STAR experiment, the Silicon Vertex Tracker (SVT), the Silicon Strip Detector (SSD) that enhances tracking capabilities of the STAR, and the Zero Degree Calorimeter (ZDC) used for monitoring, triggering and locating interaction vertices.

4 J/ψ measurements in heavy ion collisions

The first experimental study of the J/ψ production in heavy ion collisions at high energy was done at the SPS accelerator located at CERN and has been followed on by the PHENIX and STAR experiments at the RHIC.

4.1 SPS results

In SPS the J/ψ production was studied in the $\mu^+\mu^-$ decay channel. The suppression of the J/ψ production was observed in central Pb+Pb collisions at NA38.

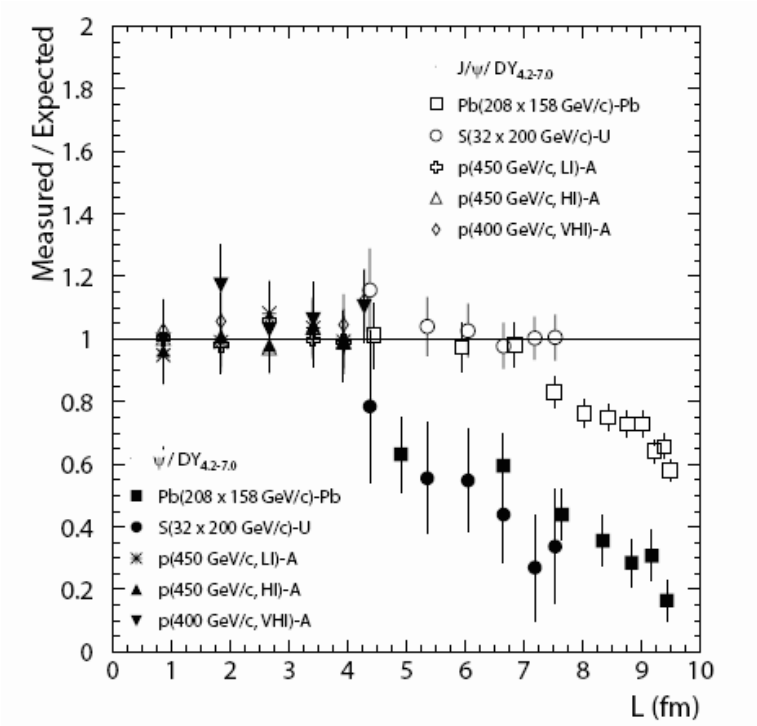

Figure 13: The ratio of measured yields to expected production of J/ψ at NA38, NA50 and NA51 experiments as a function of path length [2].

The NA50 experiment measured the J/ψ production in Pb+Pb collisions at $\sqrt{s}$=17.3GeV. Fig. 13 illustrates the comparison between measured and expected J/ψ yields as a function of the path length. The path length (L) is the total distance traveled by a nucleon through the medium. The path length increases with an increase in the collision centrality and decreases with a decrease in collision centrality. The production in peripheral Pb+Pb collisions agree up to L=4fm approximately with cold nuclear matter absorption. In more

central collisions the J/ψ production was strongly suppressed. The level of J/ψ cold nuclear matter absorption was establish from the measurements at p+A collisions [9].

The NA60 experiment studied the J/ψ production via the dimuon decay as a function of centrality distribution in In+In collisions at $\sqrt{s}$=17.3GeV. In Fig. 14 J/ψ production in In+In collisions compared with expected production when only the absorption in the cold nuclear matter is calculated are shown. A large suppression is present in collisions involving more than 80 participant nucleons [10].

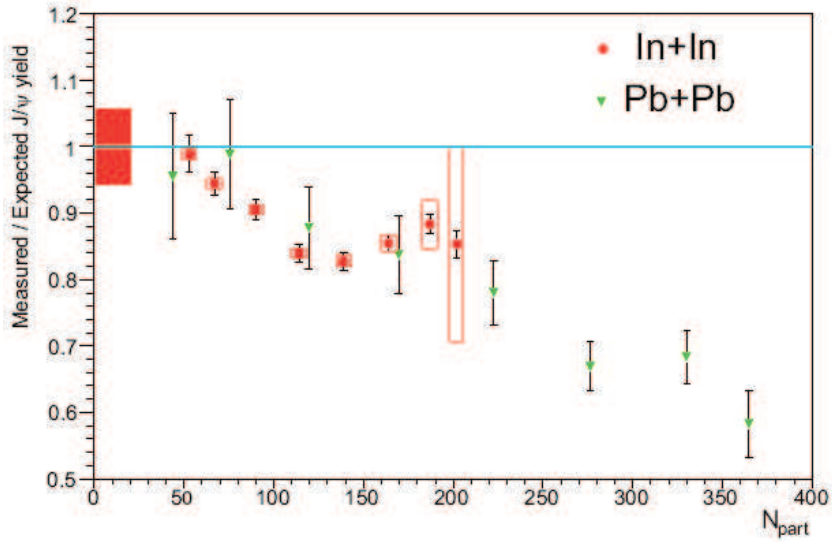

Figure 14: J/ψ suppression in In+In (NA60) and Pb+Pb (NA50) collisions as a function of a centrality [10].

These anomalous suppressions in Pb+Pb central collisions at NA50 and In+In central collisions at NA60 have been of a great interest. It was assumed that this suppressions may be a signal of a QGP formation. Before these measurements, several theoretical calculations have been done with and without the QGP formation that both have been able to match the results. This make the J/ψ suppression result inconclusive. Because of this uncertainty, the study of the J/ψ production continued at the RHIC in higher energy collisions.

4.2 RHIC results

The J/ψ production has been studied at the RHIC in p+p, Cu+Cu, d+Au, and Au+Au collisions at $\sqrt{s}$ =200GeV. The observed suppression of J/ψ in Au+Au collisions as a function of centrality is one of the evidence of the Quark Gluon Plasma formation at the RHIC. The results obtained by the PHENIX and STAR experiments will be summarized in this subsection.

PHENIX results

At the PHENIX experiment at the RHIC the J/ψ production has been measured in Au+Au and Cu+Cu collisions at $\sqrt{s}$=200GeV. J/ψs have been detected through their dielectron decay at a mid rapidity ($|y| < 0.35$), and through their dimuon decay at a forward rapidity ($1.2 < |y| < 2.4$) [11]. To establish the baseline and cold nuclear matter suppression, the J/ψ production was measured in p+p and d+Au collisions. The results from d+Au collisions are shown in Fig. 15 where the cold nuclear matter suppression is illustrated as a function of rapidity. The positive rapidity corresponds to the deuteron going direction. The rapidity(y) of the particle is defined as follows:

$$y = \frac{1}{2}\ln(\frac{E+p_z}{E-p_z}) \tag{7}$$

where E is a particle energy and p_z is a momentum in the beam direction.

The Au+Au and Cu+Cu results were compared with cold nuclear matter expectations. The J/ψ nuclear modification factor, R_{AA}, in Au+Au collisions as a function of the number of participants is shown in Fig.16. Data from SPS experiments(NA38, NA50 and NA60) are there also displayed. The R_{AA} decreases to 0.2 for the most centrality collisions.

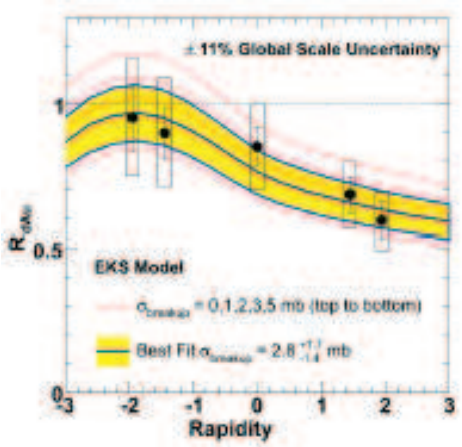

Figure 15: J/ψ R_{dA} in d+Au collisions as a function of rapidity [11].

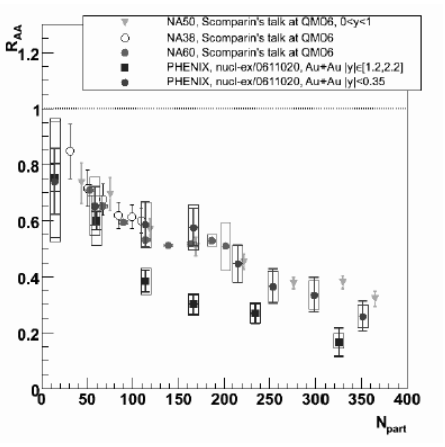

Figure 16: J/ψ R_{AA} as a function of N_{part} at RHIC compared to SPS [11].

Finally, the suppression observed at $p_T < 5$GeV/c, that is define as follows:

$$p_T = \sqrt{p_x^2 + p_y^2} \tag{8}$$

where p_x and p_y are the x and y components of momentum, at a mid rapidity is similar to that measured at SPS. This is contrary to expectations by reason that the energy density and temperature reached at RHIC is markedly higher than at SPS. It could be due to the recombination of uncorrelated $c\bar{c}$ pairs in the medium which are more abundant in higher energy collisions. Another potential occasions may be sequential dissociation of excited charmonia states, feeddown from χ_c states, or B-mesons.

STAR results

Measurements of the J/ψ production in p+p collisions at the STAR experiment aim to become the baseline measurement for a systematic study of the charmonia production. The latest result of the J/ψ production in p+p collisions at a forward rapidity using 2-cluster and 3-cluster techniques are shown in Fig.17 and in Fig.18, respectively.

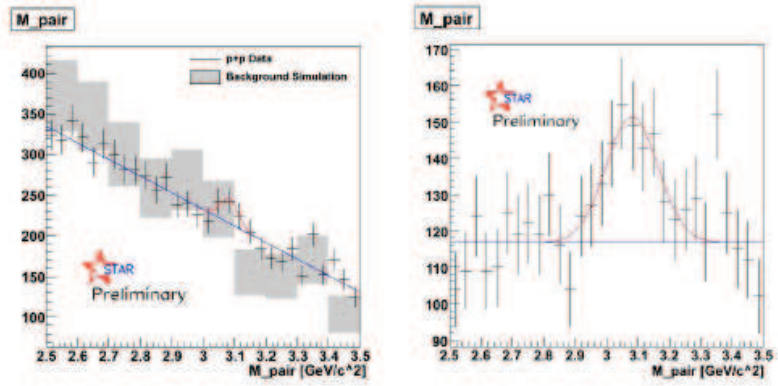

Figure 17: Invariant mass at forward rapidity in p+p collisions where the red line shows the fitted J/ψ signal, and the blue line shows the fitted background [14].

The 3-cluster analysis observes the J/ψ production through its feed-down from χ_c states ($\chi_c \rightarrow J/\psi + \gamma \rightarrow e^+ + e^- + \gamma$)[14]. In this measurements significant J/ψ signals have been reconstructed by both ways.

The J/ψ yields in d+Au collisions were reconstructed from the dielectron decay channel at a mid rapidity. The invariant mass of e^+e^- pairs at lowp_T is

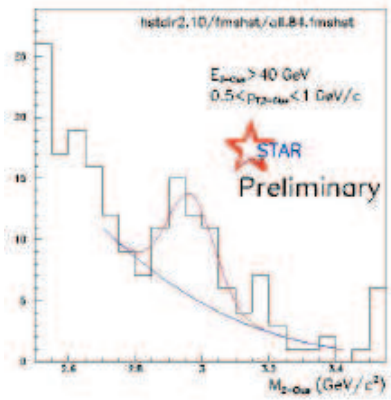

Figure 18: Invariant mass spectrum in 3-cluster analysis [14].

shown in Fig. 19, where the black line shows the reconstructed J/ψ signal, and the red line shows the background. This dataset was analyzed also in this work. The dielectron invariant mass at high p_T is illustrated in Fig. 20, where the red line shows the J/ψ signal, and the dashed line shows the background [14].

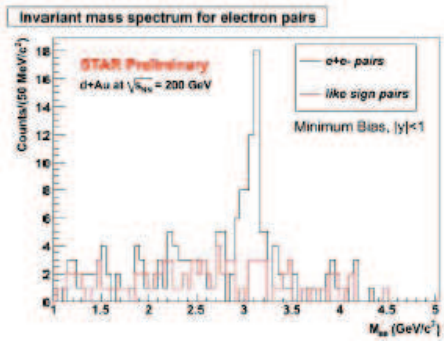

Figure 19: Dielectron invariant mass spectrum at low p_T in d+Au collisions [14].

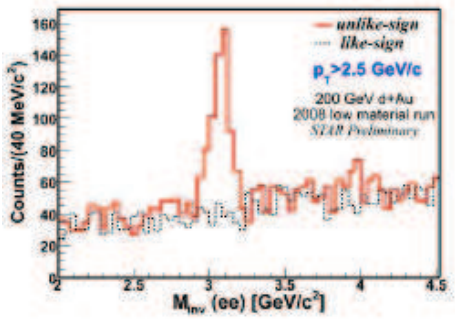

Figure 20: Dielectron invariant mass spectrum at high p_T in d+Au collisions [14].

The J/ψ production in Cu+Cu and Au+Au collisions at $\sqrt{s}$ =200GeV was measured from the e^+e^- pairs invariant mass. The mid rapidity ($|y| < 1$) results of the J/ψ production are shown in Fig. 21, where the left figure shows the dielectron invariant mass spectrum in Cu+Cu collisions before background subtraction, and the right one shows the dielectron invariant mass spectrum in Au+Au collisions after the background subtraction. The nuclear modification factor R_{AA} as a function of p_T and the centrality is shown in Fig. 22.

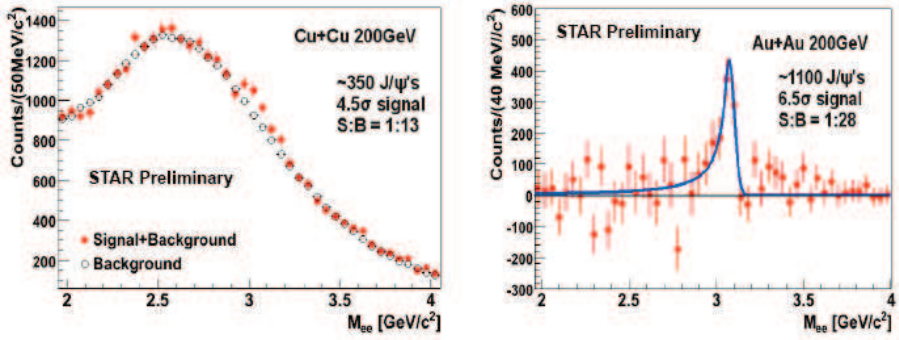

Figure 21: Invariant mass spectrum of e^-e^+ pairs in Cu+Cu collisions before the background subtraction (left) and in Au+Au collisions after the background subtraction (right) [13].

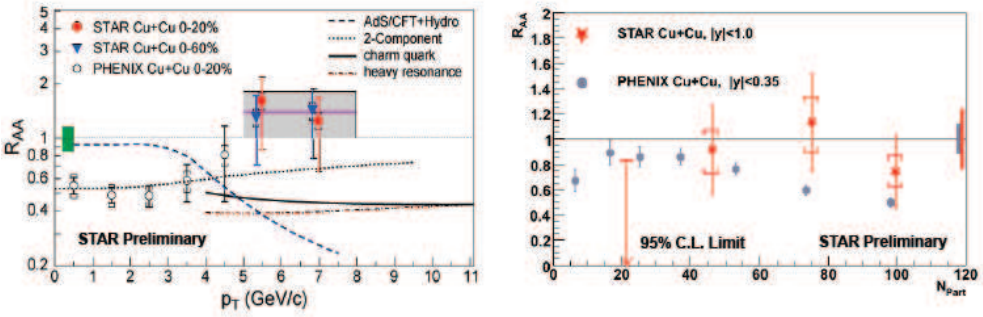

Figure 22: J/ψ R_{AA} as a function of p_T (left) and centrality (right) in Cu+Cu collisions at $\sqrt{s}$ =200GeV [17].

5 J/ψ analysis in d+Au collisions at $\sqrt{s}$=200GeV at the STAR

In this work an analysis of J/ψ production in d+Au collisions at $\sqrt{s}$=200GeV using data taken during the 2008 run with the STAR experiment at BNL is presented. The data sample was collected with a minimum bias trigger (35M events).

Events used for this analysis were that with the Z axis component of the primary vertex from -30 cm to 30 cm from the detector mid-point.

5.1 The track selection

Particle tracks are reconstructed from registered hits in the TPC readout system. The number of these fit points is the main criterium for a track quality selection. The tracks reconstructed from more than 20 points are accepted. For an elimination of double counting, another cut is used: the number of fit points over the number of maximum points (N_{Fitt}/N_{max} >0.51). The fit points cut is illustrated in Fig.23.

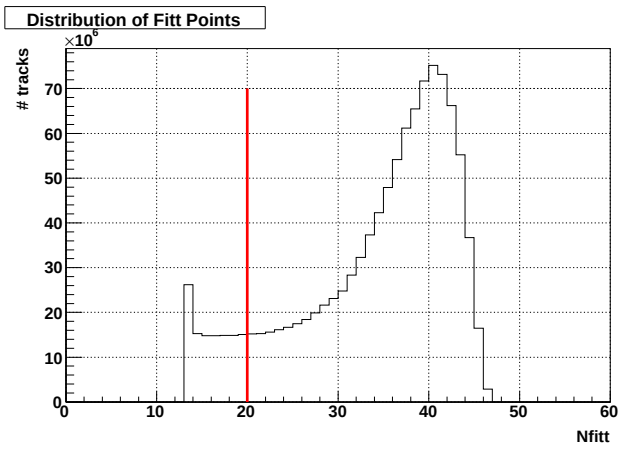

Figure 23: The fit points distribution used to the track reconstruction. The red line denotes the selection cut $N_{fitt} > 20$.

In order to eliminate a contamination from track secondary electrons, the global DCA cut (gDCA<2.0 cm) is used. The gDCA is a distance of a track to the global vertex of the event.

The J/ψ meson has a large mass, therefore the produced electrons and positrons have typicaly larger momenta than the background. Hence, the momenta cut is established to p >0.5GeV/c and p >1.0GeV/c for the second and third analysis consequently. The momentum distribution is shown in Fig. 24.

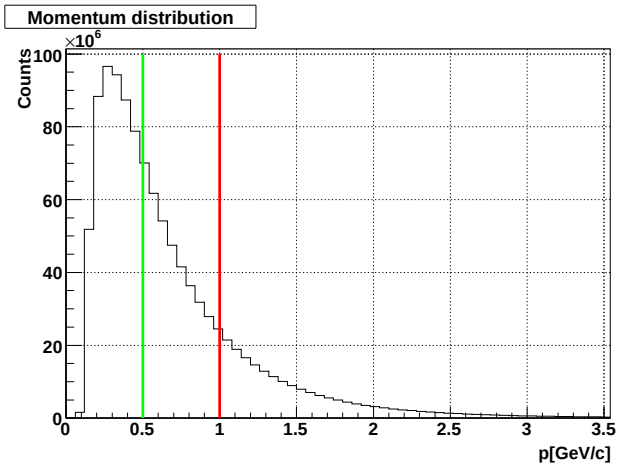

Figure 24: The momentum distribution in d+Au collisions at $\sqrt{s}$=200GeV. Green and red lines denote momentum cuts.

5.2 The electron identification

In this analysis the J/ψ signal is reconstructed from the dielectron decay channel. Therefore the main part of the analysis is to identify electrons and positrons. A charged particle is usually identified through the mass-dependent ionization energy loss dE/dx that is measured in the TPC detector. Using the dE/dx information from the TPC, particles with different mass can be distinguished. The distribution of dE/dx as a function of momentum is illustrated in Fig.25.

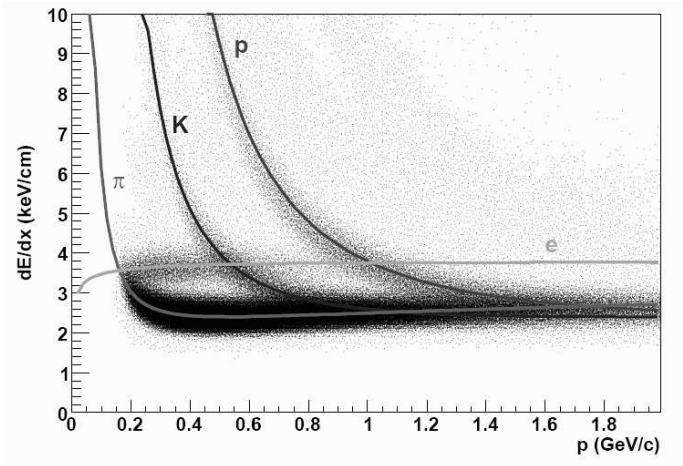

Figure 25: dE/dx as a function of the track momentum. Bichsel functions for protons (p), kaons (K), pions (Ľ), and electrons (e) are shown [16].

The dE/dx for electrons is in the range: $3 < dE/dx < 5$ keV/cm. The dE/dx distribution is shown in Fig.26, where red lines denote the upper and the lower limit of this cut.

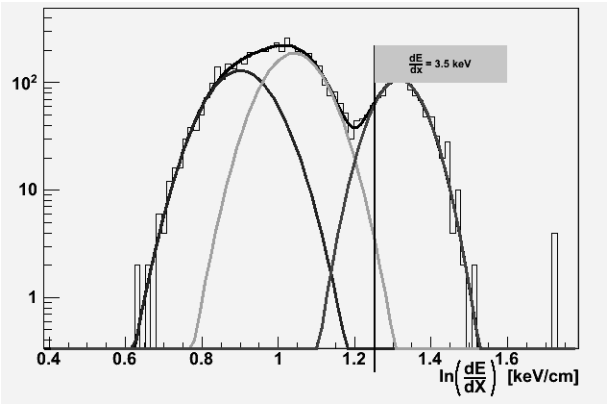

Figure 26: The projection of the dE/dx for electron sample after electron identification before dE/dx cut. Gaussian fit represents the distribution of hadrons (mainly kaons, pions for two left functions) and electrons (gaussian most to the right). The used dE/dx cut dE/dx>3.5 keV/cm is shown as a vertical line [18].

An electron cannot be identified with the TPC only due to a large hadron contamination. Then the candidates to electrons are extrapolated to BEMC towers. In the BEMC, particles deposit specific amount of their kinetic energy. Electrons deposit almost all their energy there, while hadrons deposit only its small part. The energy of the corresponding tower is taken to compute the ratio with its corresponding track momentum, p/E.

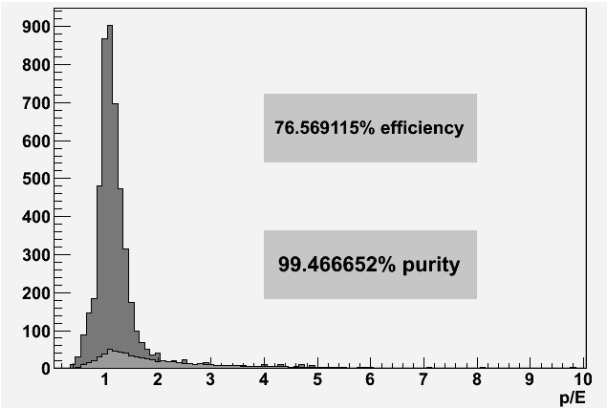

Figure 27: The p/E distribution of electron sample after electron identification before p/E cut, together with estimated hadron background [18].

Considering this fact and the ultrarelativistic state of electrons, p/E must be approximately equal to one. Then the p/E cut (0<p/E<2) can selected most electrons and reject a large amount of hadrons. In Fig. 27 the p/E distribution is shown, where the red line denotes the upper limit for the p/E cut.

Clusters are reconstructed from the SMD signal. The size of the cluster is related to the size of the electromagnetic shower. Electron showers are expected to have a wider shower profile than hadrons. To eliminate as many hadrons as few electrons as possible, the SMD cluster size cut is established to $\eta \geq 2$ and $\Phi \geq 2$. Electron candidates are tracks from the TPC that have an expected dE/dx and that can be matched with hits in the BEMC with proper parameters.

5.3 The result

The J/ψ signal in the e^+e^- decay channel is identified as a prominent peak in the dielectron invariant mass spectrum M_{inv}, calculated using the following equation:

$$M_{inv} = 2sin\frac{\theta}{2}\sqrt{p_+p_-} \tag{9}$$

where p_+ and p_- are the positron and the electron momenta, respectively, and θ is the open angle between the electron and the positron. Since $M_{J/\psi}$=3.097GeV, the estimated peak region is $2.9 < M_{J/\psi} < 3.3$.

In every event, many dielectron candidates can be reconstructed. Only some of them are the J/ψ or other decays signal, other combinations are random. These random combinations are called the combinatorial background (N_{bg}). The N_{bg} is estimated from like-signed pairs (N_{--}, N_{++}) as follows:

$$N_{bg} = N_{++} + N_{--} \tag{10}$$

Other methods as the geometric mean, the event mixing or the event rotation can be used to estimate the combinatorial background. The J/ψ signal is defined as follows:

$$N = N_{tot} - N_{bg} \tag{11}$$

The significance of the final J/ψ signal is define as:

$$sq = \frac{S}{\sqrt{(2B+S)}} \tag{12}$$

where S is the J/ψ signal after background subtraction, and B+S is the total yield of e^+e^- pairs. Also another definition is used:

$$sq' = \frac{S}{\sqrt{(B+S)}} \tag{13}$$

In order to be able to compare it with preview results, both values are listed.

Data were analyzed using three different cuts that are resumed in Tab. 2. Dielectron invariant mass distributions in d+Au at $\sqrt{s}$=200GeV collisions before and after background subtraction are shown in Fig. 28, Fig. 29 and Fig. 30, respectively. The significance of the J/ψ signal and the final signal size for a single analysis was estimated at ($sq = 3.6\sigma; sg' = 5.0\sigma; S = 222$), ($sg = 3.2\sigma; sg' = 4.4\sigma; S = 151$) and ($sg = 4.2\sigma; sg' = 5.5\sigma; S = 120$).

The signal was fitted with a gaussian function. The mean and the sigma of the gaussian fit for each analysis were found to be (3.096; 0.042)GeV, (3.078; 0.037) GeV, and (3.085; 0.049)GeV.

These results are consistent with parallel analysis of the same data sample [14].

cut	Analysis 1	Analysis 2	Analysis 3
N_{fitt}	-	> 20	> 20
Nf_{itt}/N_{max}	-	> 0.51	> 0.51
gDCA	-	< 2	< 2
dE/dx [keV/cm]	$3 < dE/dx < 5$	$3 < dE/dx < 5$	$3 < dE/dx < 5$
p/E	< 2	< 2	< 2
SMD cluster size η	≥ 2	≥ 2	≥ 2
SMD cluster size Φ	≥ 2	≥ 2	≥ 2
p [GeV/c]	-	> 0.5	> 1

Table 2: The summary of cuts used for J/ψ analyses in d+Au collisions at $\sqrt{s}$=200GeV.

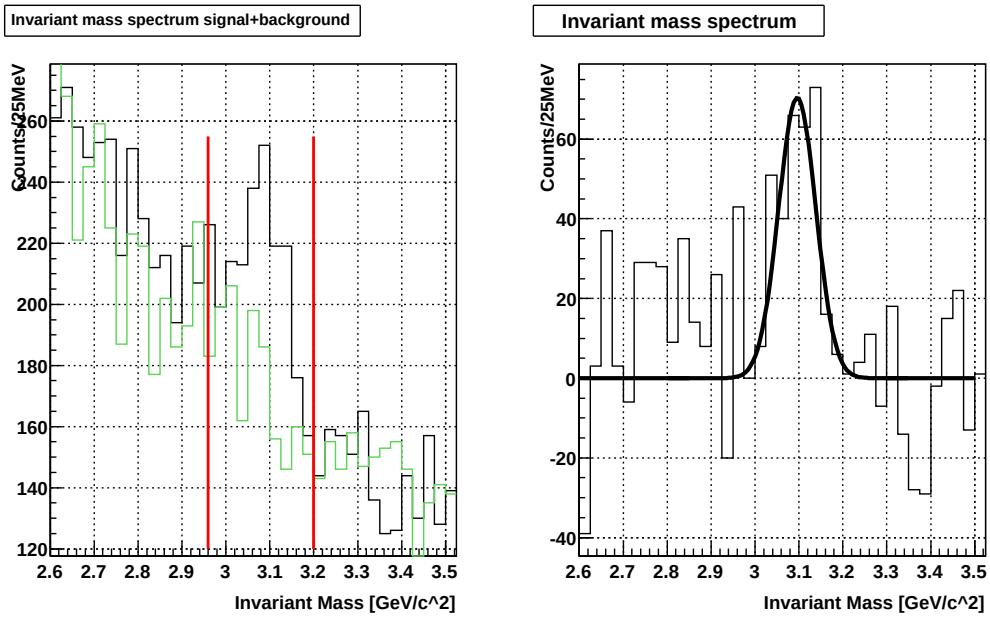

Figure 28: Cut 1: the e^+e^- invariant mass spectrum in d+Au at $\sqrt{s}$=200GeV before background subtraction on the left, and after background subtraction (background was calculated from like-sign pairs) on the right. The significance and the signal size were estimated as $(sg = 3.6\sigma; sg' = 5.0\sigma; S = 222)$. The J/ψ peak is fitted with a gaussian fit with the mean and the sigma found to be (3.096; 0.042)GeV.

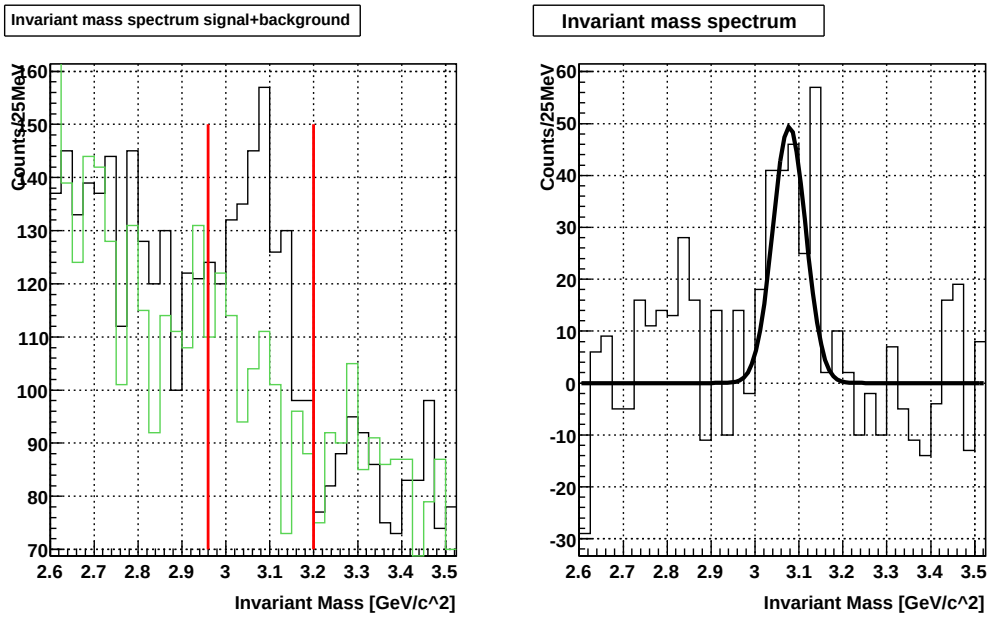

Figure 29: Cut 2: the e^+e^- invariant mass spectrum in d+Au at $\sqrt{s}$=200GeV, before background subtraction on the left, and after background subtraction (background was calculated from like-sign pairs) on the right. The significance and the signal size were estimated as ($sg = 3.2\sigma; sg' = 4.4\sigma; S = 151$). The J/ψ peak is fitted with a gaussian fit with the mean and the sigma found to be (3.078; 0.037)GeV.

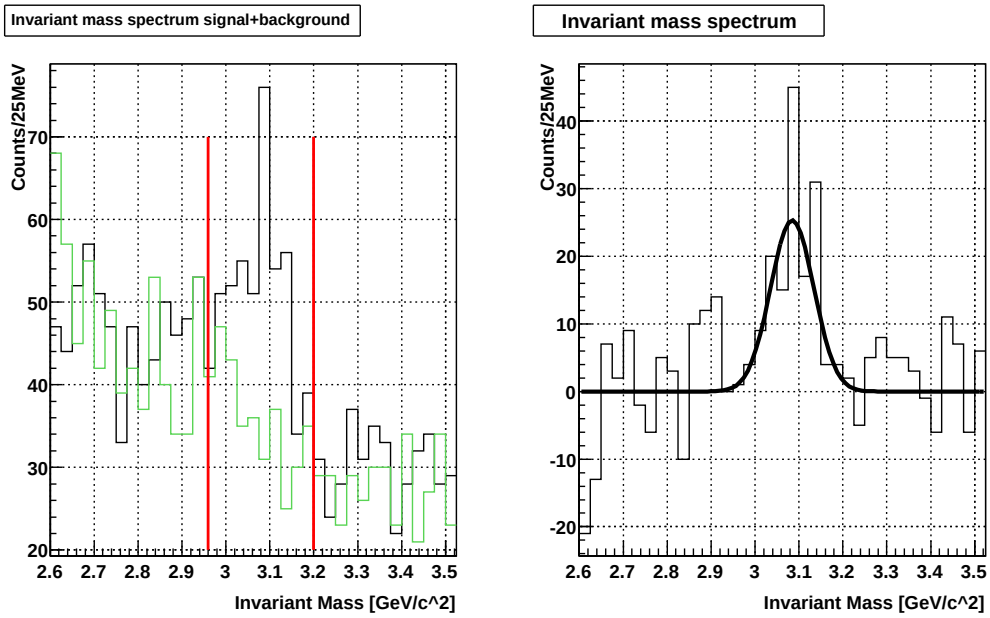

Figure 30: Cut 3: the e^+e^- invariant mass spectrum in d+Au at $\sqrt{s}$=200GeV, before background subtraction on the left, and after background subtraction (background was calculated from like-sign pairs) on the right. The significance and the signal size were estimated as ($sg = 4.2\sigma; sg' = 5.5\sigma; S = 120$). The J/ψ peak is fitted with a gaussian fit with the mean and the sigma found to be (3.085; 0.049)

6 Summary

The primary objective of this work was a study of the J/ψ production and its properties in heavy ion collisions, and a reconstruction of the J/ψ signal in d+Au collisions at $\sqrt{s}$=200GeV at the STAR. The electron-positron invariant mass spectrum was used to reconstruct J/ψs.

In this work a detailed analysis of the d+Au collisions was performed. Electrons were separated from the reconstructed tracks using the combined information of the TPC and BEMC. Dilepton pairs was constructed and random combinations were subtracted. A clear signal of J/ψ was observed. The three possible combinations of the selected criteria (cut1, cut2, cut3) was investigated. The reported significance is 4.2σ and signal is S=120.

For finalization of the results it is necessary to perform the following further studies: optimalization of signal, reduction of the errors of the combinatorial background by application of event mixing, the study of the signal reconstruction efficiency.

References

[1] G. Taku, J/ψ Production in High Energy Heavy Ion Collisions at RHIC, Dissertation thesis (2007)

[2] S. Oda, Production of Charmonia in Cu+Cu and p+p Collisions at $\sqrt{s}$=200 GeV, Dissertation thesis (2008)

[3] T. Matsui and H. Satz, Phys. Lett. B 178 416 (1986)

[4] J.K. Dong, J/ψ Production in d+Au and p+p Collisions at $\sqrt{s}$=200 GeV, Dissertation thesis (2004)

[5] R. Vogt, Ultrarelativistic heavy-ion collisions (2007)

[6] M. Harisson et al., Nucl. Instr. and Meth. A 499 235 (2003)

[7] http://www.star.bnl.gov

[8] M. Sharma, A Study of Fluctuations in Ultra-Relativistic Heavy Ion Collisions, Dissertation thesis (2008)

[9] B. Alessandro et al. (NA50 Collaboration), Eur.Phys.J.C39:335-345 (2005),arXiv:hep-ex/0412036v1

[10] R. Arnaldi et al. (NA60 Collaboration), arXiv:0706.4361v1[nucl-ex](2007)

[11] E.T. Atomssa (PHENIX Collaboration), arXiv:0805.4562v1 [nucl-ex] (2008)

[12] R.Arnaldi, Quark Matter (2009)

[13] D. Kikola (STAR Collaboration), J/ψ production in Au+Au and Cu+Cu collisions at $\sqrt{s}$ = 200 GeV at STAR, Quark Matter (2009)

[14] C. Perkins (STAR Collaboration), J/ψ Production in p+p and d+Au Collisions at $\sqrt{s}$ = 200 GeV at STAR, Quark Matter (2009)

[15] M. Anderson et al. (STAR Collaboration),Nucl.Instrum.Meth.A499:659-678 (2003), arXiv:nucl-ex/0301015v1

[16] J.E. Gonzalez, J/Psi Production in Au+Au Collisions at $\sqrt{s}$ = 200GeV, Dissertation thesis (2006)

[17] B.I. Abelev et al. (STAR Collaboration), arXiv:0904.0439v1 (2009)

[18] D. Tlustý, STAR analysis meeting, MIT (2009)